

RESEARCH ARTICLE

Investigation of CuO/ITO Photoelectrode Fabricated by PVD for Efficient Photoelectrochemical Water Splitting and Hydrogen Evolution

Muhammad Junaid¹  | Noor-ul-Ain¹ | Mohamed Sharaf² | Mohammad El-Meligy^{3,4} | Nazir Ahmad⁵

¹Institute of Physics, The Islamia University of Bahawalpur, Bahawalpur, Pakistan | ²King Saud University, Riyadh, Saudi Arabia | ³Jadara University Research Center, Irbid, Jordan | ⁴Applied Science Research Center, Applied Science Private University, Amman, Jordan | ⁵Department of Physics, Annamalai University, Annamalai Nagar, Tamil Nadu, India

Correspondence: Muhammad Junaid (mjunaid310@yahoo.com)

Received: 9 July 2024 | **Revised:** 11 October 2024 | **Accepted:** 19 October 2024

Funding: This work was supported by the King Saud University, RSPD2024R704.

Keywords: CuO | EIS | hydrogen | LSV | PVD

ABSTRACT

Hydrogen and renewable fuels were generated using cost-effective and efficient electrocatalysts for water splitting. In this work, a CuO-based photocathode is used for the water splitting to generate hydrogen energy by PVD technique. The XRD analysis reveals the deposition of CuO thin film on ITO substrates, which is monoclinic. The XRD and LSV analysis of CuO confirmed the type of semiconductor and observed to be P-type semiconductor. SEM study of CuO confirmed the shape, morphology to be a circular and regular shape. The grain size of deposited CuO thin film was found to be 18 nm. The absorption and transmission of CuO thin film were observed through UV spectroscopy analysis and were found to be better photocatalyst in visible range 415–425 nm. The transmittance of the prepared thin film was noted to be maximum 7.6% in the UV range (280–300 nm). The band gap was also measured employing the Tauc plot and found to be 2.98 eV, which is most favorable for water splitting application. FTIR study showed the stretching, vibration, and the functional group of the deposited CuO thin film; the broad band of stretching of Cu-O in monoclinic CuO was observed at the range of 500–700 cm^{-1} , and further peaks were also noted at the range of 1500–1600 cm^{-1} . The linear sweep voltammetry (LSV) of CuO thin film was calculated in the absence of solar spectra and the presence of solar spectra and observed to be enhanced in current under solar spectra. The solar light to hydrogen emission percentage (STH %) of CuO through LSV was observed to be 2.04% under solar spectra. The low Nyquist curve of blank ITO and CuO-coated ITO substrate via electrochemical impedance spectroscopy (EIS) analysis was observed, which confirmed the enhancement of EIS of CuO-coated ITO. The hydrogen generation rate was also calculated by electrochemical cell and observed to be 5325.21 mol g^{-1} for 6 h.

1 | Introduction

CuO is an inorganic compound that contains copper and oxygen. It has a blackish-brown color and is commonly found as a mineral known as tenorite. CuO is used in a variety of industrial applications, including as a catalyst, in the production of batteries, and as a pigment in ceramics and glass [1]. CuO has a variety of physical and chemical properties that make it useful in these

applications. For example, it is a semiconductor that can conduct both electricity and heat. It is also a basic oxide, which means it can react with acids to form salts. In terms of its potential applications in energy storage, CuO has been investigated as a potential electrode material for lithium-ion batteries. Some research has shown that CuO could offer an increased energy density and cycle life compared to other common electrode materials. However, there are still challenges that need to be overcome in

terms of the stability and performance of CuO-based electrodes [2]. Copper's polyvalency causes it to generate a variety of oxides; the most well-known of which are cupric oxide (CuO) and cuprous oxide (Cu₂O), which are p-type semiconductors due to copper vacancies in the lattice. Cupric oxide (CuO), commonly known as tenorite, is the most stable phase in the copper oxide family. It exhibits excellent optical absorbance, a reported narrow bandgap energy of 1.8 to 3 eV, and the capacity to synthesis in many nanostructured morphologies. CuO has recently received a lot of attention in thin-film technology due to its abundance in the Earth's crust, environmentally friendly nature, and tailorable electro-optical properties. These applications include solar cells, electrochemical devices, and, most importantly, gas sensors [3].

In photocatalytic applications, CuO is chosen over Cu₂O due to its higher stability and lower bandgap [4], which allows its optical bandgap to be tuned by appropriate metal doping to utilize a wide spectrum of visible (solar/synthetic) radiations. The strong reactivity of copper (Cu²⁺) combined with CuO's narrow bandgap makes it a viable photocatalyst for water purification. The electrons in the conduction band are unstable in phase pure CuO; therefore, the majority of photo-generated electrons migrate to the valance band and recombine with the hole without participating in the oxidation process. Photocatalysis efficiency can therefore be increased by delaying charge carrier recombination [5].

In energy conversion, copper oxide thin films are used as photocatalysts in water-splitting reactions, where they can use light to split water molecules into hydrogen and oxygen. This makes copper oxide nanoparticles an important material for the production of clean hydrogen fuel [5] Overall, CuO is an important material in various industrial and research applications due to its unique properties and potential benefits.

Farhad et al. [6] has done a great deal of research on the affordable, reliable, and productive electrocatalysts for photoelectrochemical water-splitting to find a resolution to the world's energy issue over the past 10 years. One of the few photocatalysts

with a limited bandgap, CuO is a potential photocathodic catalyst thanks to its intriguing physicochemical features. Under synthetic direct solar radiation, this photocatalyst exhibits high efficiency for the PEC hydrogen evolution process. Here, the most recent developments in CuO-based photoelectrodes, particularly undoped, doped, and CuO composites, are thoroughly examined in the context of PEC water-splitting. Additionally, every classification's characterization, core characteristics, and other elements are thoroughly explained. In addition to the unique features of CuO-based photocatalysts, the physicochemical properties of CuO/2D materials as sections of developing nanocomposites in photocurrent-generating equipment are investigated in distinct parts. For the CuO heterostructure photocathodes in particular, the PEC water splitting implementation is studied, and each group's characteristics, including electronic configuration, imperfections, bandgaps, and institutional arrangements, are carefully evaluated [7].

Farhad et al. [8] analyze the treatment of organic, inorganic, and microbiological contaminants in water and wastewater; heterogeneous photocatalysis is a promising method. Due to its low cost, environmental friendliness, ability to operate at ambient conditions of pressure and temperature, and capacity to entirely disintegrate toxins into ecologically sound products under the right circumstances, it is a procedure that is preferred over other conventional wastewater treatment strategies. In photocatalytic degradation, active ions produced in situ and their immediate assault when intense radiation strikes the semiconductor catalyst are the major causes of the degradation of organic pollutants. As a result, the used catalyst should be highly photonic efficient, less poisonous, plentiful, chemically and photo catalytically safe, and visible light active to effectively and economically remove wastewater contaminants [8]. One of these potential challenges is the photocatalytic efficiency of copper oxide (CuO), which has been limited primarily by the fast dispersion and poor mobility of photogenerated charge carriers. The techniques used to address the aforementioned limitations are summarized in this study, along with additional

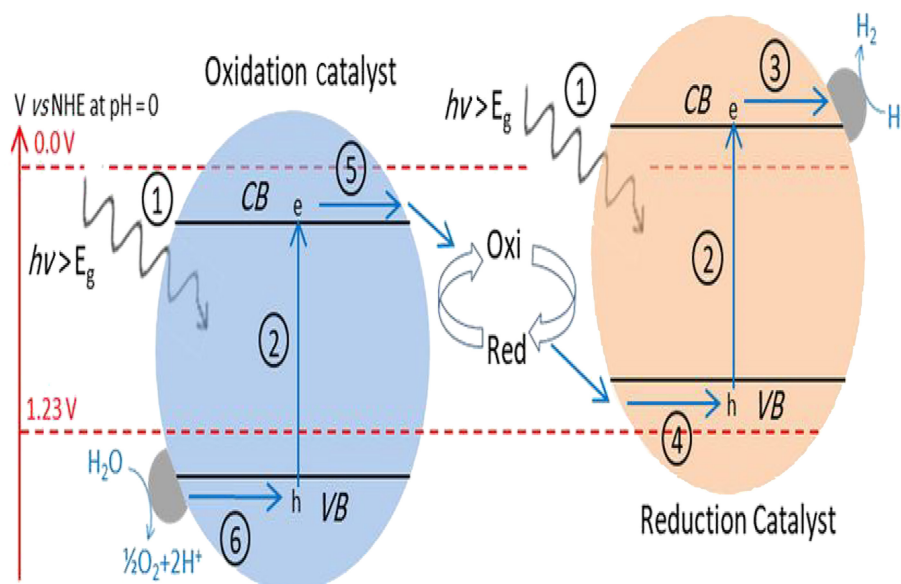


FIGURE 1 | Water splitting mechanism of CuO-based photocatalyst for H₂ generation [12].

operational factors that will increase its catalytic performance for the removal of harmful organic and inorganic metal ions from aqueous environments [9–11].

Water splitting mechanism is mentioned in Figure 1.

2 | Experimental Procedure

2.1 | CuO Thin Film Preparation

The first step in preparing the heterostructure thin film was to deposit CuO on an ITO substrate using thermal vapor deposition. Initially, clean the substrate with ethanol. The starting material for the formation of the CuO thin film was 0.5 g of 99% pure CuO powder from Sigma Aldrich. The tungsten boat contained 99% pure CuO [13]. The tungsten boat and substrate holder (made up of brass) were fixed at a distance of 19 cm in the working chamber. This working chamber is a metal envelope that houses a vacuum system, material evaporation, and deposition of vapors on the substrate, which is placed at the top of the boat. Now, we turned on the power supply and switched on the Rotary Van Pump. It takes up to 45 min for proper work. At the same time, we turn on the water supply. Subsequently, the diffusion pump heater was turned on to warm up the oil [14, 15]. Now, we opened the roughing valve until it showed a reading of 10^{-2} mbar. Open the backup valve after closing the roughing valve. Finally, link the diffusion pump and vacuum chamber by opening the isolation valve (Baffle Valve), achieving a vacuum of 10^{-5} mbar switched on the power source of the transformer and applying a current of 75–85 A to electrically heat the tungsten boat containing CuO till 250°C. With the application of thermal energy, the source material was evaporated on 1000°C and deposited on the substrates. After the deposition, close the baffle valve and turn off the diffusion pump, let the rotary van pump and backing valve run for a while, close the backing valve and shut off the rotary van pump, off the main power, and let the water supply run until the temperature of the flowing water returned to normal. A very fine thin film of CuO was deposited at the rate of 0.1–10 Å/s on the borosilicate and indium tin oxide substrates with film thickness 10–500 nm due to the sublimation of CuO [16]. The surface profilometer is used for the measurements of thickness of the thin film at room temperature and found to be average 1 nm. High temperatures can alter film properties and make measurements challenging. Surface profilometers have limited resolution (~1–10 nm). Thin films are degraded, oxidize, and diffuse at 1000°C–1200°C, affecting thickness measurements. Surface profilometers may not maintain accuracy at high temperatures due to thermal expansion, instrument drift, or damage.

3 | Experimental Analysis

The physical and chemical properties of the samples were evaluated using various analytical techniques. X-ray diffraction (XRD) was used to determine their structural properties, whereas Nova Nano SEM was used to analyze their morphological properties. Spectrophotometry was used to measure their optical properties. To assess their ability to split water through photoelectrochemical [17] reactions, the samples were used as working electrodes

in a three-electrode electrochemical cell, with platinum and Ag/AgCl electrodes as the counter and reference electrodes, respectively [18]. The experiments were carried out in a 0.5 M Na_2SO_4 electrolyte solution with a pH of 7; a 100-W xenon arc lamp with an AM 1.5G filter was used to simulate solar spectra. Linear sweep voltammetry (LSV) was performed with and without illumination at a scan rate of 10 mV/s. A 100 mL 0.5 M Na_2SO_4 solution, a quartz reactor, and a gas chromatograph were used to test photocatalytic hydrogen production in the presence of the samples. A standard procedure was used to quantify the hydrogen produced during the photocatalytic reaction [19].

To prepare for the photocatalytic reaction, nitrogen was used to purge the solution 30 to 60 min before the experiment to remove any dissolved oxygen species from the flask. The photocatalyst was placed 16 cm away from the xenon lamp. A gas chromatograph equipped with a thermal conductivity detector (Clarus 500 PerkinElmer, United States) was used to measure photocatalytic hydrogen production. The hydrogen production rate was recorded at hourly intervals for a total of 10 h for each sample, in addition to the measurement of oxygen produced [20, 21]. To determine the weight of the deposited films, the weight of the substrate was subtracted from the combined weight of the substrate and the deposited films.

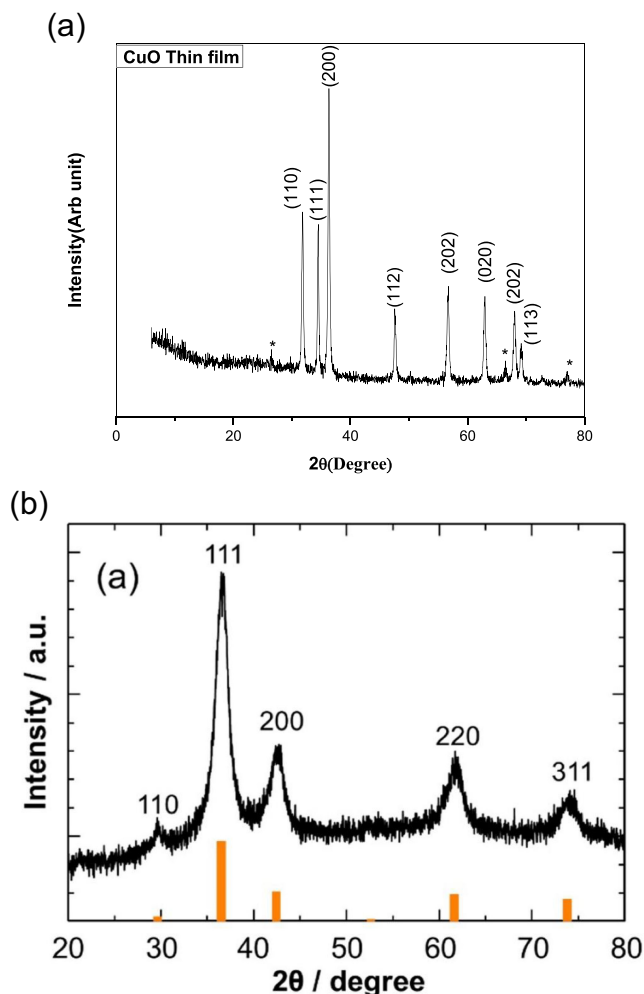


FIGURE 2 | (a) XRD patterns of deposited CuO thin film on ITO substrate. (b) Standard JCPDS #05-0661 for monoclinic CuO [23].

3.1 | XRD Study

The confirmation of CuO thin film XRD spectra was acquired using a Bruker D8 Advance powder X-ray diffractometer with Cu K α ($\lambda=1.5406 \text{ \AA}$) radiation. The diffraction patterns were recorded using a step size of ~ 0.0250 and a duration per step of 18 s. The samples were rotated to ensure homogeneous observations. A D-8 Bruker diffractometer work on 40 kV and 40 mA, from 0° to 80° (2θ), is mentioned in Figure 2a [22].

The XRD pattern of the deposited CuO thin film (Figure 2a) exhibits characteristic peaks matching the monoclinic crystal structure of CuO (JCPDS #05-0661). The observed peaks at 2θ values of 32.48° , 35.46° , 38.74° , 48.72° , 53.48° , 58.26° , 61.54° , 66.28° , and 68.12° correspond to the (110), (002), (111), (-202), (020), (202), (-113), (311), and (220) planes, respectively. The absence of additional peaks corresponding to Cu (JCPDS #04-0836)

or Cu₂O (JCPDS #05-0667) phases confirms the phase purity of the deposited CuO thin film.

For comparison, the XRD pattern of pure CuO powder (Sigma Aldrich) is shown in Figure 2, demonstrating excellent agreement with the deposited film. The standard JCPDS #05-0661 pattern is also included (Figure 2b) for Reference [23], and there is no extra peak observed except ITO peaks as cited by an asterisk (*).

The deposition of CuO film is homogeneous in thickness and has a reddish-gray appearance. As a result, the deposition time was set at 2 h to meet the requirement of uniformity with increased thickness. The variation in thickness was discovered to be correlated with the variation in deposition potentials 0.355, 0.455, and 0.555 V, and its value is between 2 and $2.3 \mu\text{m}$. Crystallinity affects charge carrier mobility and surface reaction

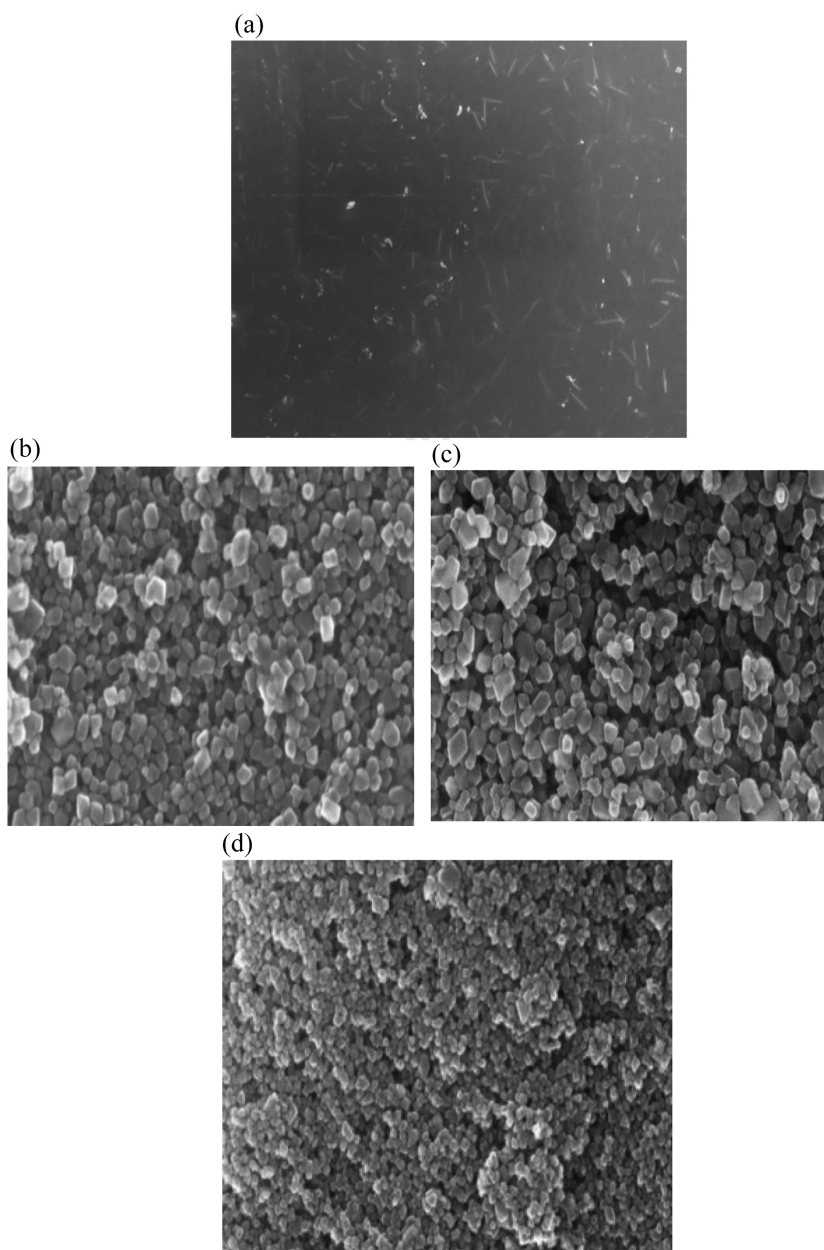


FIGURE 3 | (a) SEM analysis of ITO substrate. (b, c, d) SEM analysis of CuO on ITO substrate.

kinetics. Phase purity influences the availability of active sites for catalysis [24].

3.2 | SEM Study

The SEM (Cube II Emcraft South Korea) setup is used to analyze ITO substrates; it typically exhibits a smooth, featureless surface. ITO films consist of small grains (10–50 nm) that are not visible in SEM images. The surface roughness of ITO substrates is usually low, around 1–5 nm. ITO has a polycrystalline structure, but individual crystals are not easily visible in SEM as shown in Figure 3a.

CuO studied at different scales gives the symmetrical circular shape of the obtained thin films; the particles are compactly arranged due to the agglomeration [25]. The grain size of the

CuO thin films was measured through ImageJ software and found to be about 18 to 30 nm with a mean surface area of $15.7 \text{ m}^2/\text{g}$ [26].

The grain size, shape, and agglomeration of particles in Figure 3b–d were noted as the magnification scale increased. The symmetrical grain size and low particle size are responsible for the better PEC response toward UV solar spectra [27].

The surface plot analysis was performed using ImageJ software to determine the surface smoothness of the CuO, and dark surfaces have a low albedo, absorbing more sunlight at the range of 1–100 nm [28]. The surface smoothness is also responsible for the maximum absorption of solar spectra, which generate more electron–hole pairs for better photocatalysis as cited in Figure 4.

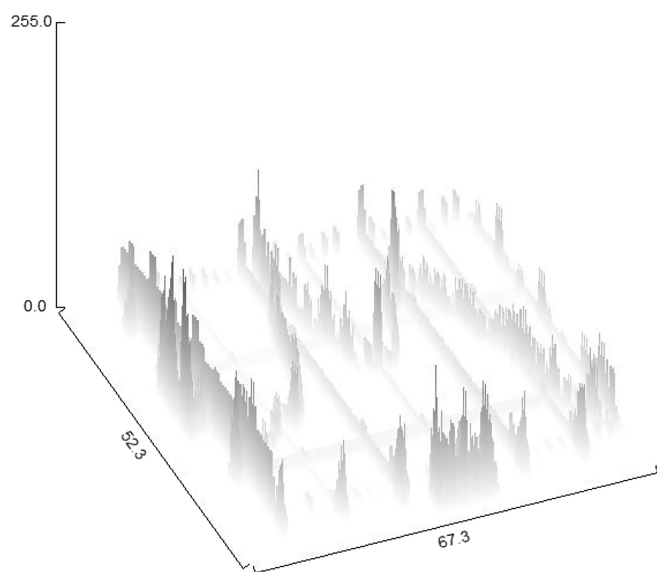


FIGURE 4 | Surface plot of CuO.

3.3 | FT-IR Analysis

FTIR (Thermo Scientific Nicolet iS 5, United States) is used for identifying functional groups within the structure of molecules. It utilizes unique energy absorption bands associated with specific chemical bonds to analyze structural details and bonding properties for intricate molecules [29]. Significant discoveries may be seen in the FTIR spectrum of the freshly manufactured copper oxide sample material displayed in Figure 5.

CuO has a limited number of vibrational modes in the range of $400\text{--}1000 \text{ cm}^{-1}$. FTIR instruments typically have lower sensitivity and resolution at high wavenumbers. FTIR detectors have a cutoff wavelength around $400\text{--}1000 \text{ cm}^{-1}$, making it difficult to detect peaks at lower wavelengths. Water vapor and CO_2 in the air absorb radiation in the high-wavenumber region mask potential peaks. The bands seen at 1107.29 and $31,358.61 \text{ cm}^{-1}$ indicate the vibrations associated with the stretching of the O–H bond [30]. Two different bands were found at 868.29 and 2003.14 cm^{-1} in the examination of the FTIR spectra of CuO thin films within the range of 500 to 4000 cm^{-1} , which correspond to certain CuO modes. The peak at 868.29 cm^{-1} shows the stretching vibration of Cu–O bonds in one direction, whereas the high-frequency peak at 610 cm^{-1} likely suggests the stretching vibration of Cu–O bonds in the other direction [31]. Peaks at 1438 , 2498.08 , and 3433.48 cm^{-1} show different bending vibrational modes in the Cu–O bond, in addition to their existence.

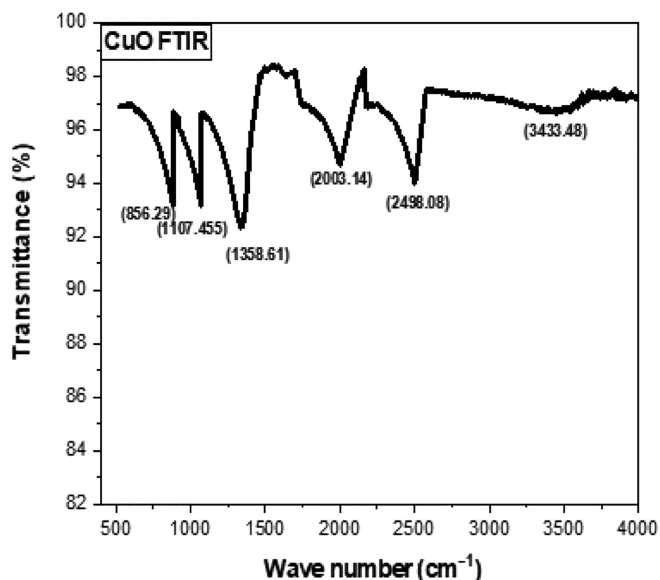


FIGURE 5 | FTIR spectrum of CuO thin film.

3.4 | UV-Vis Spectroscopy

A UV-VIS-NIR spectrophotometer (Shimadzu UV2600 plus) equipped with an integrating sphere was used to assess the optical absorption and transmission of films produced on quartz substrates. The absorbance of CuO was measured via UV spectroscopy and noted the maximum absorbance in the visible range (violet-blue region) of solar spectra at the range of wavelength from 415 to 425 is about 7.6 , whereas the absorbance is recorded minimum at the wavelength below from 415 nm range as mentioned in Figure 6. This range of wavelength (<400) of solar spectra is a better range to absorb visible range of solar

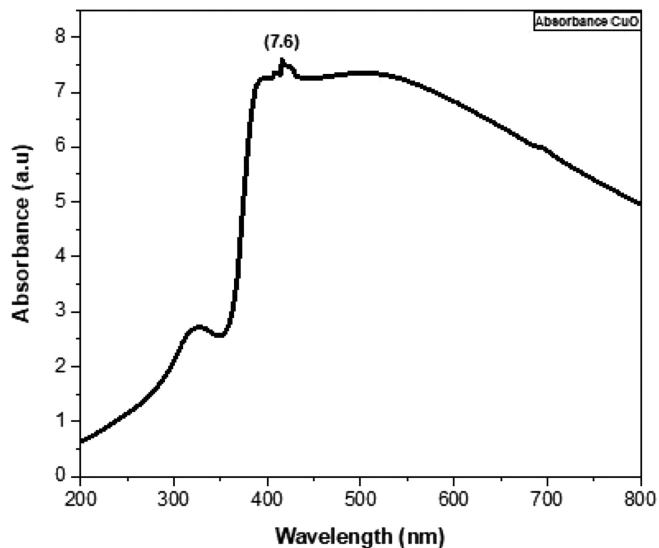


FIGURE 6 | UV spectroscopy of CuO.

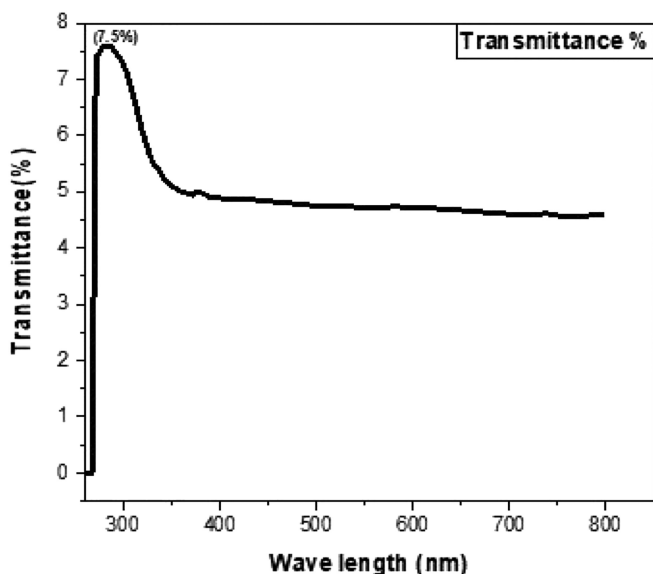


FIGURE 7 | Transmittance of CuO thin film.

spectra for the maximum generation of PEC, and solar spectra at these wavelength ranges are used for water splitting to generate hydrogen energy, and the voltage needed for water splitting is being used as a solar spectrum [32, 33].

The transmittance % of CuO was noted through UV spectroscopy and found to be 7.5% in UV region and gradually decreases with increasing of wavelength, which is very better for the solar application to split water for the production of hydrogen energy as shown in Figure 7. The low transmittance in visible region is the evidence of better photocurrent.

3.5 | Bandgap Determination

The optical bandgap of the deposited sample on ITO was determined using a Tauc plot constructed from diffuse reflection

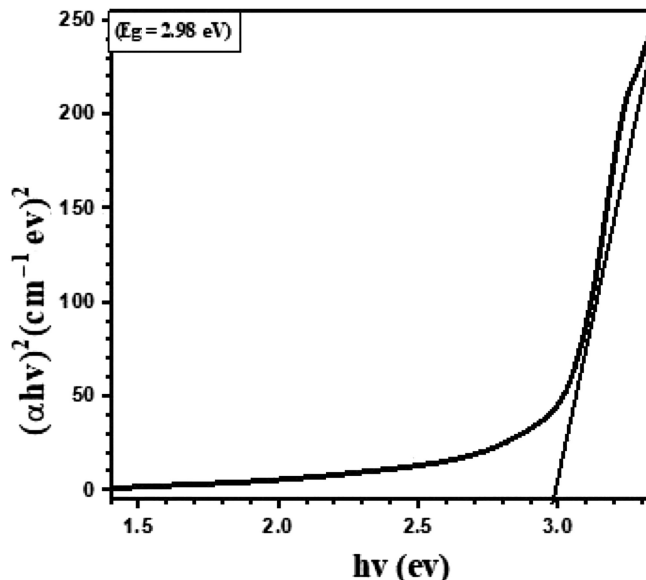


FIGURE 8 | Band gap measurement of CuO.

data using the K-M function, as shown in Figure 8. The bandgaps (E_g) of CuO thin films are determined to be 2.98 eV. The lower optical bandgap for film suggests that oxygen vacancies (V_o) create defect states in the bandgap, resulting to a reduced effective bandgap. The optical spectra of the prepared thin film of CuO were used to estimate the band gap value [34]. Knowing the thickness of the obtained thin film, the optical absorption coefficient (α) is determined through the mentioned formula:

$$\alpha = 1/d \ln(1/T). \quad (1)$$

Here, d denotes the thickness of the thin films in use whereas T stands for their transmittance [35]. The absorption coefficient is affected by the strong zone of photon energy absorbed by thin films, and the band gap of metal oxide semiconductors is measured using the well-known Tauc relation.

$$(\alpha hv) = \beta (hv - E_g)^\eta \quad (2)$$

β is the constant and η powers are taken $\frac{1}{2}$ for indirect band gap semiconductors and 2 for the direct band gap semiconductors [36].

The CuO band gap of 2.98 eV is the most favorable band gap to absorb visible range of solar spectra for better photocatalytic activity to generate hydrogen energy via water splitting [37].

3.6 | Electrochemical Impedance Spectroscopy (EIS) Study

The EIS measurements were carried out in the dark using a potentiostat (Autolab, PGSTAT-30) with a frequency analyzer. To maintain the stability of the CuO film, an AC signal with an amplitude of 20 mV and frequencies ranging from 50 Hz to 10 kHz

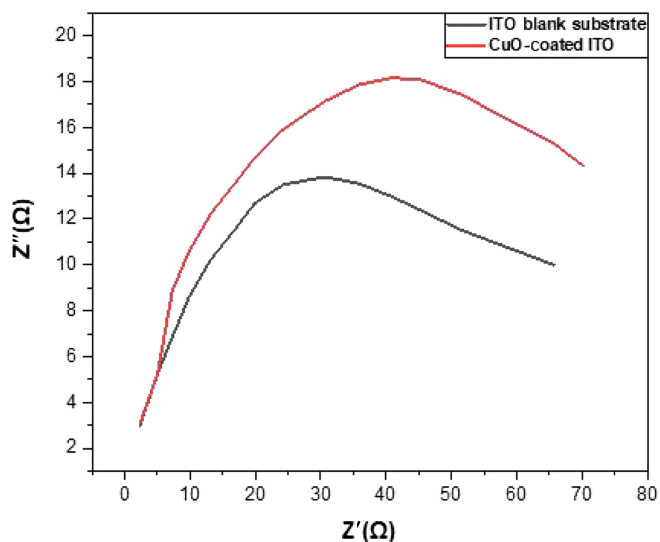


FIGURE 9 | Nyquist plot for CuO-coated ITO and blank ITO Substrate.

was delivered over a limited potential window at a constant bias voltage.

EIS was carried out for insight into the reaction kinetics. The semicircle in the impedance spectra in the Nyquist plot shows the resistance transfer of charge [38, 39]. The diameter of the semicircle showed the reaction kinetics.

A smaller diameter of the Nyquist plot showed faster reaction kinetics. The low diameter of the plotted graph is the confirmation of the fast reaction and low resistance, which is a very better application for photocurrent generation by absorbing the solar spectra as reported in Figure 9 [40, 41]. CuO-coated ITO substrate has maximum EIS values compared to blank ITO substrate due to charge transfer resistance (R_{ct}), pseudocapacitive behavior, and enhanced surface roughness, whereas blank ITO substrate has lower EIS values due to smoother surface, lower charge transfer resistance, and reduced pseudocapacitance. The blank ITO has lower EIS values ($\approx 100\text{--}500\ \Omega$), and CuO-coated ITO has higher EIS values ($\approx 1\text{--}10\ \text{k}\Omega$).

3.7 | LSV Measurements

Linear sweep voltammetry (LSV) measurements were taken in the dark using an Autolab Potentiostat (PGSTAT-30) with a frequency analyzer. To maintain the stability of the CuO film, an AC signal with an amplitude of 20 mV and frequencies ranging from 50 Hz to 10 kHz was delivered over a limited potential window at a constant bias voltage. The linear sweep voltammetry graph of the CuO thin film was examined, in which the photocurrent of the CuO thin film was calculated [42–44]. The solar light hydrogen conversion efficiency of the obtained sample CuO thin film was measured through the following reaction:

$$STH\% = \frac{(1.23 - V_{bias})J}{P} \times 100 \quad (3)$$

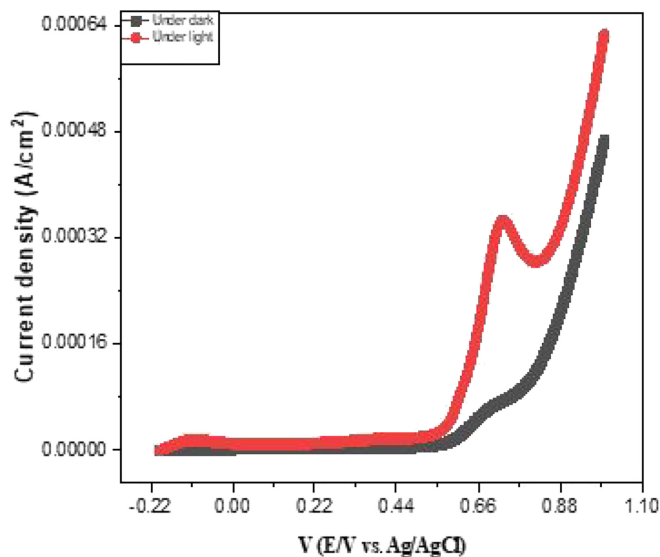


FIGURE 10 | LSV measurements of CuO thin film.

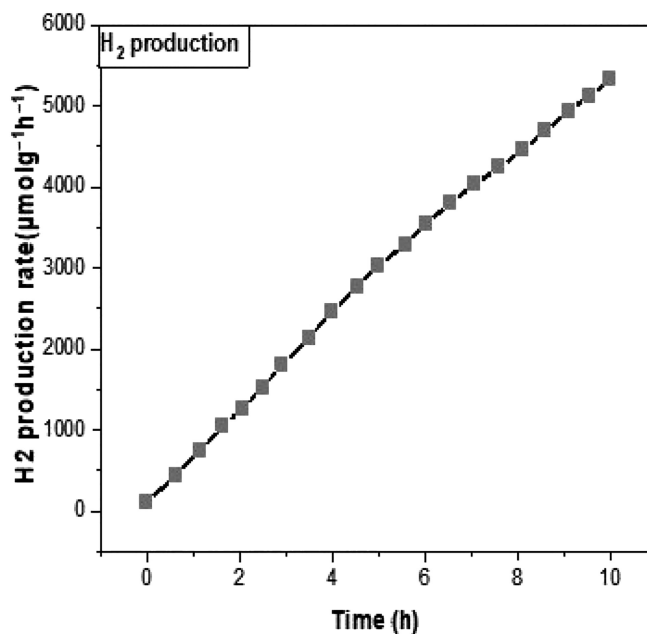


FIGURE 11 | Hydrogen production rate versus time.

V_{bias} is the applied voltage using solar spectra between the working and reference electrodes (AgCl/Ag), J is the photocurrent density, and P is the solar intensity at the Earth's surface ($100\ \text{mW}/\text{cm}^2$) [45].

The STH% of CuO thin film was measured to be 2.09% at 0.9 V, which is quite a better percentage of hydrogen generation as compared to the other semiconductors reported in the literature as shown in Figure 10 [46, 47].

The change in photocurrent under dark conditions and light conditions was measured through the below formula:

$$J = J_{light} - J_{Dark} \quad (4)$$

3.8 | Hydrogen Generation Measurement

Photoelectrochemical (PEC) water splitting is a potential method of hydrogen synthesis. The performance of PEC water splitting is largely dependent on the qualities of the light source. The UV-Vis range is 200–500 nm, and the intensity range is 10–100 mW/cm². Irradiance intensity ranges from 100 to 1000 W/m². Common light sources used in PEC water-splitting research include xenon lamps, LED arrays (UV, blue, or white LEDs), solar simulators, and laser sources (e.g., 365 or 405 nm) [48–50].

CuO is a p-type semiconductor that has a direct band gap, so the conduction band is more negative than the ITO substrate; the contact of CuO and ITO substrate creates a p-n junction, which is the cause of the electric field [51, 52]. The electrons of CuO migrate to react with water to generate hydrogen, whereas the holes are consumed by the sacrificial agent as mentioned in Figure 11.

The hydrogen production rate of CuO under a xenon lamp was noted to be 5325.21 mol·g⁻¹·h⁻¹, which is higher than other materials [12, 53].

4 | Conclusion

CuO was successfully deposited on ITO substrate using PVD techniques for photocatalytic hydrogen production activity via potentiogalvanostat. The XRD confirmed the deposition of CuO on ITO substrates using an X-ray diffractometer, and some extra peaks of ITO also observed and compared it with blank ITO substrate. The surface profilometer is used for the measurements of thickness of the thin film at room temperature and found to be average 1 nm. SEM study revealed the morphology and grain size of the CuO, which was a symmetrical circular shape and grain size of 18 to 30 nm. It is also observed more clarity in grain size with the increasing of resolution till 200 nm. The surface plot was examined through imageJ software and to be found smooth, which is favorable for maximum absorption of solar spectra for hydrogen generation. FTIR peaks are not observed in the 400–750 cm⁻¹ region because the lower sensitivity in this region, too thickness of thin film is also affected peak visibility. It is also due to substrate material KBr absorb in this region. The instrument background is also one of the reasons and noted the distortion in rest of the peaks. The UV spectroscopy confirmed the absorption of solar spectra in the visible range, and the band gap was also measured using a Tauc plot for better conditions while exposed to solar spectra. The C₂₁H₂₅C₁₀O₅ (Epon 828, Bisphenol A-type epoxy) in making photoelectrodes common insulation materials Epoxy resins (e.g., Epon 828, Araldite) is used. The exposed areas for CuO photoelectrodes range from 0.1 to 1 cm², and the window materials used in photoelectrochemical cells are quartz. The electrochemical impedance spectroscopy confirmed the better conduction state and gave the minimum impedance for blank ITO substrate and maximum for CuO-coated ITO due to charge transfer resistance (R_{ct}), pseudocapacitive behavior, and enhanced surface roughness, whereas blank ITO substrate has lower EIS values due to smoother surface, lower charge transfer resistance, and reduced pseudocapacitance. The linear

sweep voltammetry of CuO was studied while exposed to solar spectra and found to be enhanced; the solar light to hydrogen emission STH% was 2.09% at 0.9 V. The hydrogen evolution of CuO under solar spectra was examined and recorded as 5325.21 mol·g⁻¹·h⁻¹.

Author Contributions

Muhammad Junaid: conceptualization, methodology, investigation, validation, software, formal analysis, visualization, writing – original draft. * **Noor-ul-Ain:** supervision. **Mohamed Sharaf:** project administration, funding acquisition, investigation. **Mohammad El-Meligy:** funding acquisition, validation, investigation. **Nazir Ahmad:** data curation.

Acknowledgments

The authors extend their appreciation to King Saud University, Saudi Arabia, for funding this work through Researchers Supporting Project number (RSPD2024R704), King Saud University, Riyadh, Saudi Arabia.

Conflicts of Interest

The authors declare no conflicts of interest.

Data Availability Statement

The data that support the findings of this study are available on request from the corresponding author. The data are not publicly available due to privacy or ethical restrictions.

References

1. A. M. Musa, S. F. Farhad, M. A. Gafur, and A. T. Jamil, “Effects of Withdrawal Speed on the Structural, Morphological, Electrical, and Optical Properties of CuO Thin Films Synthesized by Dip-Coating for CO₂ Gas Sensing,” *AIP Advances* 11, no. 11 (2021): 1150041, <https://doi.org/10.1063/5.0060471>.
2. S. F. Farhad, R. F. Webster, and D. Cherns, “Electron Microscopy and Diffraction Studies of Pulsed Laser Deposited Cuprous Oxide Thin Films Grown at Low Substrate Temperatures,” *Materialia* 3 (2018): 230–238, <https://doi.org/10.1016/j.mtla.2018.08.032>.
3. M. R. Islam, M. Saiduzzaman, S. S. Nishat, A. Kabir, and S. F. Farhad, “Synthesis, Characterization and Visible Light-Responsive Photocatalysis Properties of Ce Doped CuO Nanoparticles: A Combined Experimental and DFT+ U Study,” *Colloids and Surfaces A: Physicochemical and Engineering Aspects* 617 (2021): 126386, <https://doi.org/10.1016/j.colsurfa.2021.126386>.
4. S. F. Farhad, M. M. Hossain, M. S. Bashar, N. I. Tanvir, and S. Islam, “Communication—Texture and Bandgap Tuning of Phase Pure Cu₂O Thin Films Grown by a Simple Potentiostatic Electrodeposition Technique,” *ECS Advances* 3 (2024): 013001, <https://doi.org/10.1149/2754-2734/ad2f46>.
5. M. Dey, N. K. Das, M. Dey, S. F. U. Farhad, M. A. Matin, and N. Amin, “Impact of Source to Substrate Distance on the Properties of Thermally Evaporated CdS Film,” *International Journal of Renewable Energy Research (IJRER)* 11, no. 1 (2021): 495–503, <https://doi.org/10.20508/ijrer.v11i1.11627.g8168>.
6. S. F. Farhad, D. Cherns, J. A. Smith, N. A. Fox, and D. J. Fermin, “Pulsed Laser Deposition of Single Phase n-and p-Type Cu₂O Thin Films With low Resistivity,” *Materials & Design* 193 (2020): 108848, <https://doi.org/10.1016/j.matdes.2020.108848>.
7. S. F. Farhad, S. Majumder, M. A. Hossain, N. I. Tanvir, R. Akter, and M. A. Patwary, “Effect of Solution pH and Post-Annealing Temperatures

- on the Optical Bandgap of the Copper Oxide Thin Films Grown by Modified SILAR Method,” *MRS Advances* 4, no. 16 (2019): 937–944, <https://doi.org/10.1557/adv.2019.139>.
8. S. F. Farhad, M. A. Hossain, N. I. Tanvir, et al., “Structural, Optical, Electrical, and Photoelectrochemical Properties of Cuprous Oxide Thin Films Grown by Modified SILAR Method,” *Materials Science in Semiconductor Processing* 95 (2019): 68–75, <https://doi.org/10.1016/j.mssp.2019.02.014>.
9. M. S. Habib, S. F. Farhad, N. I. Tanvir, et al., “Fabrication and Characterization of Graphene-Barium Titanate-Graphene Layered Capacitors by Spin Coating at low Processing Temperatures,” *ECS Journal of Solid State Science and Technology* 12, no. 9 (2023): 093006, <https://doi.org/10.1149/2162-8777/acf4be>.
10. A. BaQais, M. W. Alam, M. Farhan, G. Muteeb, N. Allag, and S. Mushtaq, “Probe-Sonicated Synthesis of CuO–ZnO Hybrid Nanocomposite for Photocatalytic and Supercapacitor Applications,” *Inorganics* 11, no. 9 (2023): 370.
11. W. Alam, M. U. Khatoun, and A. Qurashi, “Synthesis and Characterization of Cu-SnO₂ Nanoparticles Deposited on Glass Using Ultrasonic Spray Pyrolysis and Their H₂S Sensing Properties,” *Current Nanoscience* 8, no. 6 (2012): 919–924.
12. M. Junaid, Noor-Ul-Ain, and W. Q. Khan, “Bandgap Alignment of Solar-Driven Multilayers Metal Oxide Thin Film for Water Splitting to Generate Hydrogen Energy,” *International Journal of Hydrogen Energy* 52 (2023): 199–208, <https://doi.org/10.1016/j.ijhydene.2023.06.161>.
13. M. W. Alam, H. S. al Qahtani, H. Albalawi, et al., “Enhanced Electrodes for Supercapacitor Applications Prepared by Hydrothermal-Assisted Nano Sheet-Shaped MgCo₂O₄@ ZnS,” *Crystals* 12, no. 6 (2022): 822.
14. K. Rudresha, A. Z. Hussain, C. R. Ravikumar, et al., “Structural, Electrochemical Sensor and Photocatalytic Activity of Combustion Synthesized of Novel ZnO Doped CuO NPs,” *Materials Research Express* 10, no. 7 (2023): 075005.
15. Y. Iwamura, T. Itoh, J. Kasagi, S. Murakami, and M. Saito, “Excess Energy Generation Using a Nano-Sized Multilayer Metal Composite and Hydrogen gas,” *Journal of Condensed Matter Nuclear Science* 33, no. 1 (2020): 1–13.
16. H. Ferhati, F. Djeflal, and A. Benhaya, “Optimized High-Performance ITO/Ag/ITO Multilayer Transparent Electrode Deposited by RF Magnetron Sputtering,” *Superlattices and Microstructures* 129 (2019): 176–184.
17. H. Ferhati, F. Djeflal, A. Bendjerad, A. Benhaya, and A. Saidi, “Perovskite/InGaAs Tandem Cell Exceeding 29% Efficiency via Optimizing Spectral Splitter Based on RF Sputtered ITO/Ag/ITO Ultra-Thin Structure,” *Physica E: Low-dimensional Systems and Nanostructures* 128 (2021): 114618.
18. S.-F. Zheng, J. S. Hu, L. S. Zhong, W. G. Song, L. J. Wan, and Y. G. Guo, “Introducing Dual Functional CNT Networks Into CuO Nanomicrospheres Toward Superior Electrode Materials for Lithium-Ion Batteries,” *Chemistry of Materials* 20, no. 11 (2008): 3617–3622.
19. B. Trembach, A. Grin, M. Turchanin, N. Makarenko, O. Markov, and I. Trembach, “Application of Taguchi Method and ANOVA Analysis for Optimization of Process Parameters and Exothermic Addition (CuO-Al) Introduction in the Core Filler During Self-Shielded Flux-Cored Arc Welding,” *The International Journal of Advanced Manufacturing Technology* 114, no. 3–4 (2021): 1099–1118.
20. S. Naz, A. Gul, M. Zia, and R. Javed, “Synthesis, Biomedical Applications, and Toxicity of CuO Nanoparticles,” *Applied Microbiology and Biotechnology* 107 (2023): 1039–1061, <https://doi.org/10.1007/s00253-023-12364-z>.
21. R. Siavash Moakhar, S. M. Hosseini-Hosseiniabad, S. Masudy-Panah, et al., “Photoelectrochemical Water-Splitting Using CuO-Based Electrodes for Hydrogen Production: A Review,” *Advanced Materials* 33, no. 33 (2021): 2007285.
22. A. K. Sibhatu, G. K. Weldegebrieal, S. Imteyaz, S. Sagadevan, N. N. Tran, and V. Hessel, “Synthesis and Process Parametric Effects on the Photocatalyst Efficiency of CuO Nanostructures for Decontamination of Toxic Heavy Metal Ions,” *Chemical Engineering and Processing Process Intensification* 173 (2022): 108814.
23. K. Mikami, Y. Kido, Y. Akaishi, A. Quitain, and T. Kida, “Synthesis of Cu₂O/CuO Nanocrystals and Their Application to H₂S Sensing,” *Sensors* 19 (2019): 211, <https://doi.org/10.3390/s19010211>.
24. Q. Zhang, K. Zhang, D. Xu, et al., “CuO Nanostructures: Synthesis, Characterization, Growth Mechanisms, Fundamental Properties, and Applications,” *Progress in Materials Science* 60 (2014): 208–337.
25. A. K. Sibhatu, G. K. Weldegebrieal, S. Sagadevan, N. N. Tran, and V. Hessel, “Photocatalytic Activity of CuO Nanoparticles for Organic and Inorganic Pollutants Removal in Wastewater Remediation,” *Chemosphere* 300 (2022): 134623.
26. H. Absike, Z. Essalhi, H. Labrim, et al., “Synthesis of CuO Thin Films Based on Taguchi Design for the Solar Absorber,” *Optical Materials* 118 (2021): 111224.
27. H. Chang, M. J. Kao, K. C. Cho, S. L. Chen, K. H. Chu, and C. C. Chen, “Integration of CuO Thin Films and Dye-Sensitized Solar Cells for Thermoelectric Generators,” *Current Applied Physics* 11, no. 4 (2011): S19–S22.
28. S. Jesumathy, M. Udayakumar, and S. Suresh, “Experimental Study of Enhanced Heat Transfer by Addition of CuO Nanoparticle,” *Heat and Mass Transfer* 48 (2012): 965–978.
29. K. Phiwdang, S. Suphankij, W. Mekprasart, and W. Pecharapa, “Synthesis of CuO Nanoparticles by Precipitation Method Using Different Precursors,” *Energy Procedia* 34 (2013): 740–745.
30. S. Y. Lee, Y. S. Park, and T.-Y. Seong, “Optimized ITO/Ag/ITO Multilayers as a Current Spreading Layer to Enhance the Light Output of Ultraviolet Light-Emitting Diodes,” *Journal of Alloys and Compounds* 776 (2019): 960–964.
31. P. K. Namburu, D. P. Kulkarni, D. Misra, and D. K. Das, “Viscosity of Copper Oxide Nanoparticles Dispersed in Ethylene Glycol and Water Mixture,” *Experimental Thermal and Fluid Science* 32, no. 2 (2007): 397–402.
32. M. Chandrasekar, M. Subash, S. Logambal, et al., “Synthesis and Characterization Studies of Pure and Ni-Doped CuO Nanoparticles by Hydrothermal Method,” *Journal of King Saud University, Science* 34, no. 3 (2022): 101831.
33. S. Jiebing, R. Xiong, S. Wang, W. Tang, H. Tong, and J. Shi, “Preparation and Characterization of Molybdenum Oxide Thin Films by Sol-Gel Process,” *Journal of Sol-Gel Science and Technology* 27 (2003): 315–319.
34. I. Shaheen and K. S. Ahmad, “Modified sol-Gel Synthesis of MoO₃ NPs Using Organic Template: Synthesis, Characterization and Electrochemical Investigations,” *Journal of Sol-Gel Science and Technology* 97 (2021): 178–190.
35. E. Arulkumar, S. Thanikaikarasan, and N. Tesfie, “Influence of Deposition Parameters for Cu₂O and CuO Thin Films by Electrodeposition Technique: A Short Review,” *Journal of Nanomaterials* 2023 (2023): 8987633, 19 pages, <https://doi.org/10.1155/2023/8987633> Dar M., et al., Structural and magnetic properties of CuO nanoneedles synthesized by hydrothermal method. *Applied Surface Science*, 2008. 254(22): p. 7477–7481.
36. S. Kamila and V. Venugopal, “Synthesis and Structural Analysis of Different CuO Nanoparticles,” *International Journal of Applied Science and Engineering* 14, no. 3 (2017): 133–146.
37. N. R. Dhineshabu, V. Rajendran, N. Nithyavathy, and R. Vetumpe-
rumal, “Study of Structural and Optical Properties of Cupric Oxide Nanoparticles,” *Applied Nanoscience* 6 (2016): 933–939.

38. J. Singh, G. Kaur, and M. Rawat, "A Brief Review on Synthesis and Characterization of Copper Oxide Nanoparticles and Its Applications," *Journal of Bioelectronics and Nanotechnology* 1, no. 1 (2016): 9.
39. Y. Abboud, T. Saffaj, A. Chagraoui, et al., "Biosynthesis, Characterization and Antimicrobial Activity of Copper Oxide Nanoparticles (CONPs) Produced Using Brown Alga Extract (Bifurcaria Bifurcate)," *Applied Nanoscience* 4 (2014): 571–576.
40. R. Ranjbar-Karimi, A. Bazmandegan-Shamili, A. Aslani, and K. Kaviani, "Sonochemical Synthesis, Characterization and Thermal and Optical Analysis of CuO Nanoparticles," *Physica B: Condensed Matter* 405, no. 15 (2010): 3096–3100.
41. P. Mallick and S. Sahu, "Structure, Microstructure and Optical Absorption Analysis of CuO Nanoparticles Synthesized by Sol-Gel Route," *Nanoscience and Nanotechnology* 2, no. 3 (2012): 71–74.
42. P. Kumar, M. Chandra Mathpal, J. Prakash, B. C. Viljoen, W. D. Roos, and H. C. Swart, "Band gap Tailoring of Cauliflower-Shaped CuO Nanostructures by Zn Doping for Antibacterial Applications," *Journal of Alloys and Compounds* 832 (2020): 154968.
43. M. A. Rafea and N. Roushdy, "Determination of the Optical Band gap for Amorphous and Nanocrystalline Copper Oxide Thin Films Prepared by SILAR Technique," *Journal of Physics D: Applied Physics* 42, no. 1 (2008): 015413.
44. A. A. Radhakrishnan and B. B. Beena, "Structural and Optical Absorption Analysis of CuO Nanoparticles," *Indian Journal of Advances in Chemical Science* 2, no. 2 (2014): 158–161.
45. Y. K. Jeong and G. M. Choi, "Nonstoichiometry and Electrical Conduction of CuO," *Journal of Physics and Chemistry of Solids* 57, no. 1 (1996): 81–84.
46. M. Ates, M. A. Serin, I. Ekmen, and Y. N. Ertas, "Supercapacitor Behaviors of Polyaniline/CuO, Polypyrrole/CuO and PEDOT/CuO Nanocomposites," *Polymer Bulletin* 72 (2015): 2573–2589.
47. S. D. Jagadale, A. M. Teli, S. V. Kalake, A. D. Sawant, A. A. Yadav, and P. S. Patil, "Functionalized Crown Ether Assisted Morphological Tuning of CuO Nanosheets for Electrochemical Supercapacitors," *Journal of Electroanalytical Chemistry* 816 (2018): 99–106.
48. H. S. Park, C.-Y. Lee, and E. Reisner, "Photoelectrochemical Reduction of Aqueous Protons With a CuO/CuBi₂O₄ Heterojunction Under Visible Light Irradiation," *Physical Chemistry Chemical Physics* 16, no. 41 (2014): 22462–22465.
49. C. Seitz, S. Werner, R. Marschall, and B. M. Smarsly, "Electrospun CuO Nanofibre Assemblies for H₂S Sensing," *Zeitschrift für Physikalische Chemie* 233, no. 1 (2018): 105–116.
50. D. R. Kumar, D. Manoj, and J. Santhanalakshmi, "Optimization of Site-Specific Adsorption of Oleylamine Capped CuO Nanoparticles on MWCNTs for Electrochemical Determination of Guanosine," *Sensors and Actuators B: Chemical* 188 (2013): 603–612.
51. S. F. Farhad, M. I. Naher, N. I. Tanvir, M. S. Quddus, S. A. Jahan, and M. A. Shaikh, "Facile Top-Down Synthesis of Phase-Pure and Tunable Bandgap CuBi₂O₄ Photocathode Materials by Low-Energy Sequential Ball Milling," *ACS Applied Energy Materials* 7, no. 19 (2024): 8278–8287, <https://doi.org/10.1021/acsaem.4c01518>.
52. E. Ding, J. Hai, T. Li, et al., "Efficient Hydrogen-Generation CuO/Co₃O₄ Heterojunction Nanofibers for Sensitive Detection of Cancer Cells by Portable Pressure Meter," *Analytical Chemistry* 89, no. 15 (2017): 8140–8147.
53. T. Hussain, M. Junaid, and H. A. Qayyum, "Preparation of Ba-Doped SrTiO₃ Photocatalyst by Sol-Gel Method for Hydrogen Generation," *Chemical Physics Letters* 754 (2020): 137741, ISSN 0009-2614, <https://doi.org/10.1016/j.cplett.2020.137741>.